Drift-Time Properties of CEBAF Hall A Vertical Drift Chambers

by

Risa H. Wechsler

Submitted to the Department of Physics
in partial fulfillment of the requirements for the degree of

Bachelor of Science in Physics

at the

MASSACHUSETTS INSTITUTE OF TECHNOLOGY

June 1996

Author .....
Department of Physics
May 17, 1996

Certified by .....
Dr. Jeffrey Templon
Thesis Supervisor

Certified by .....
William Bertozzi
Professor of Physics
Thesis Supervisor

Accepted by .....
Professor June Matthews
Senior Thesis Coordinator

Drift-Time Properties of CEBAF Hall A Vertical Drift Chambers

by

Risa H. Wechsler

Submitted to the Department of Physics
on May 10, 1996, in partial fulfillment of the
requirements for the degree of
Bachelor of Science in Physics.

Abstract

In this thesis, the drift chamber simulation program `GARFIELD` was used to perform a variety of simulations of the performance of the CEBAF HALL A Vertical Drift Chamber. The focus was on simulation of the drift-time properties of the chamber. Two algorithms for path reconstuction from drift-time measurements are developed from the simulations and discussed.

Thesis Supervisors: Dr. Jeffrey Templon and Professor William Bertozzi

Drift-Time Properties of CEBAF Hall A Vertical Drift Chambers

by

Risa H. Wechsler

Submitted to the Department of Physics
on May 10, 1996, in partial fulfillment of the
requirements for the degree of
Bachelor of Science in Physics.

Abstract

In this thesis, the drift chamber simulation program `GARFIELD` was used to perform a variety of simulations of the performance of the CEBAF HALL A Vertical Drift Chamber. The focus was on simulation of the drift-time properties of the chamber. Two algorithms for path reconstuction from drift-time measurements are developed from the simulations and discussed.

Thesis Supervisors: Dr. Jeffrey Templon and Professor William Bertozzi

Acknowledgments

First I would like to thank Jeff, for all of his tireless efforts. He has taught me basically everything I know (and probably will *ever* want to know) about drift chambers. He has always been available, patient with my lack of understanding, encouraging of my work...the list goes on. I could not have asked for a better mentor. His editing of this thesis was also invaluable. Any errors that remain, of course, are my own.

I would like to thank my advisor, Professor Bertozzi, for everything he's done for me the past four years, for supporting me through this project, for hours worth of advice, for his help in editing this thesis, and for putting up with me giving him a few bruises.

Nilanga was a wonderful teacher of the fine points of building a VDC, when I first began this project. Shalev Gilad has also helped me in numerous ways throughout this project. Thanks to Craig, for providing me with part of Figure 3-1.

I would like to thank Rob Veenhof, for writing a great program, that formed the basis of most of this thesis. I would also like to thank him for helping me understand and deal with problems with the program early on.

Lastly I would like to thank Amory, Josie, and Brian, for putting up with me and keeping me sane all year long.

Contents

List of Figures

Chapter 1

Introduction

Our understanding of nuclear matter, which makes up virtually all of the world around us, is still in an elementary state. The Continuous Electron Beam Accelerator Facility (CEBAF), is a new research facility in Newport News, VA, at the forefront of current research in nuclear physics. CEBAF will use a 4-GeV electron beam in three experimental halls, and will be dedicated to basic research in Nuclear Physics using electrons as projectiles. CEBAF combines a high duty-cycle with a high-energy beam in the few-GeV range to allow a new domain of coincidence studies at high energy and momentum transfers.

Hall A of CEBAF contains two high resolution spectrometers, and will be the premier facility worldwide for studies of the $(e, e'p)$ reaction. The high-quality beam and spectrometers allow for high-precision electromagnetic coincidence experiments, from which precise separations of structure functions can be obtained.

The $(e, e'p)$ program in general requires very good resolution in the momentum and angle of detected reaction products. The detector package of each spectrometer contains two vertical drift chambers (VDCs), which are multi-wire proportional counters that are able to provide very accurate position information (see Bertozzi *et al* [2] for a good introduction to vertical drift chambers). The VDCs will be placed in the focal plane of the spectrometers to detect the trajectory of scattered high-energy particles (see Figure 1-1).

The drift chambers each consist of two planes of very thin sense wires held at

Figure 1-1: The CEBAF Hall A Spectrometer, and the placement of the VDCs in the focal plane of the beam[4].

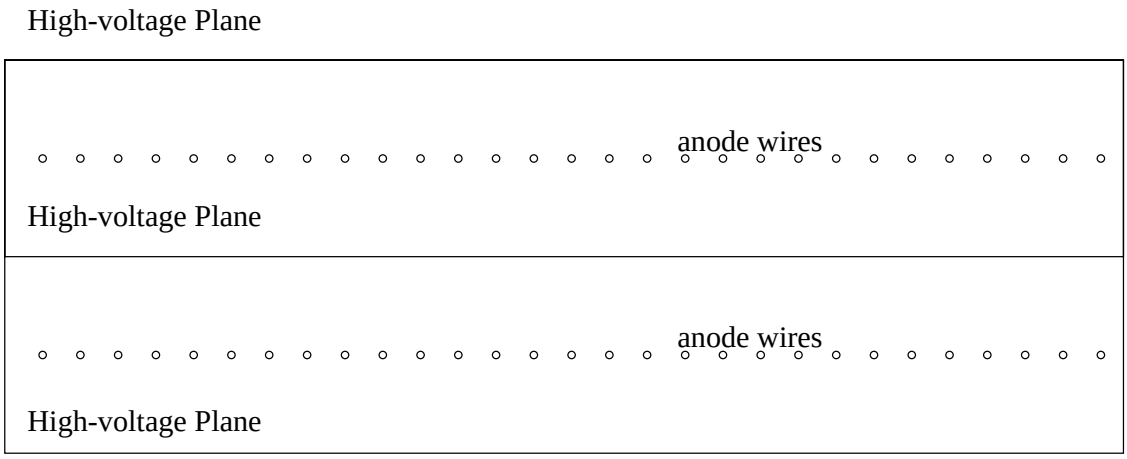

Figure 1-2: A portion of the Vertical Drift Chamber is shown, drawn to scale. The wire spacing is .423 cm, and the spacing between the wire planes and each of the high voltage planes is 1.3 cm. Note that this figure shows only a cross-section of the chamber, and that the wires in the top plane are oriented 90 degrees to those in the bottom plane. This is shown more explicity in Figure 3-2.

ground potential, positioned between high-voltage planes (Figure 1-2). They are filled with a gas that can be ionized by a high-energy charged particle incident upon the chamber. When such a particle traverses the chamber, it collides with gas molecules and liberates "drift" electrons; this is known as the primary ionization.

At the high-voltage planes, an electric field is created in the drift chamber that is perpendicular to the wire plane. This field is constant through most of the drift area, but near the thin wires it becomes closer to a purely radial $(1/r)$ field. This is shown in Figure 1-3; voltage contour plots of the chamber are shown in Figure 1-4. The liberated electrons drift along these field lines with a nearly constant velocity. Once a drift electron enters the region of increasing field, it eventually acquires enough energy to create secondary ionizations in the gas. The process repeats with the secondary electrons, which creates an avalanche effect in the region of the wire. The separation of the positive and negative charges of this avalanche creates a signal in the sense wire.

The VDCs are oriented so that the incident particle will enter at an angle with respect to the chamber. As it traverses the chamber it will then cross several cells, thus

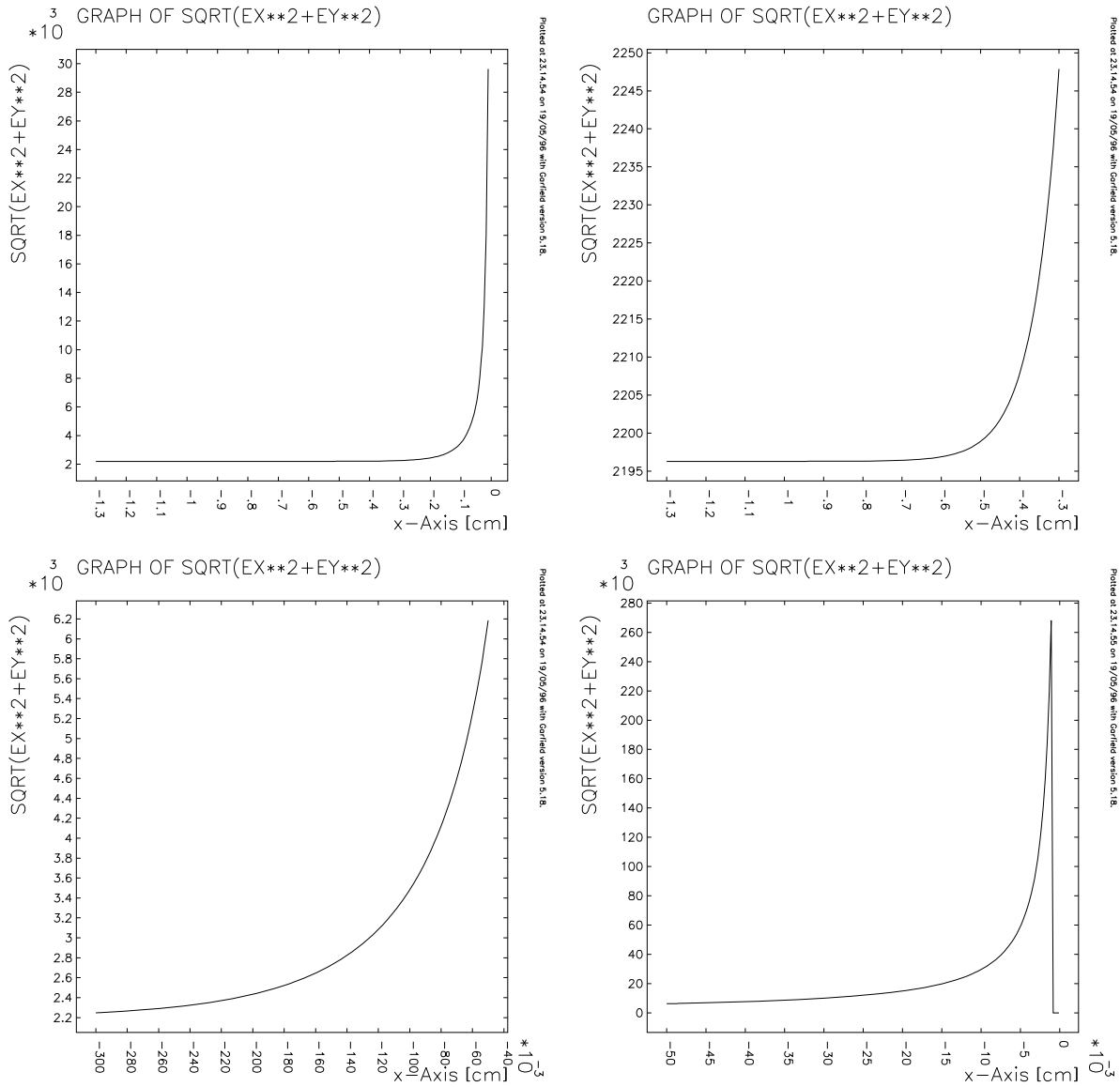

Figure 1-3: The magnitude of the electric field, in V/cm, is given as a function of perpendicular distance from the wire plane, along an axis through the wire. The first figure shows the field across the whole drift distance. The second figure shows the outer drift region of approximately constant field, and the bottom two figures show the region closer to the wire, where the field increases rapidly. The voltage on the HV planes is -4100V.

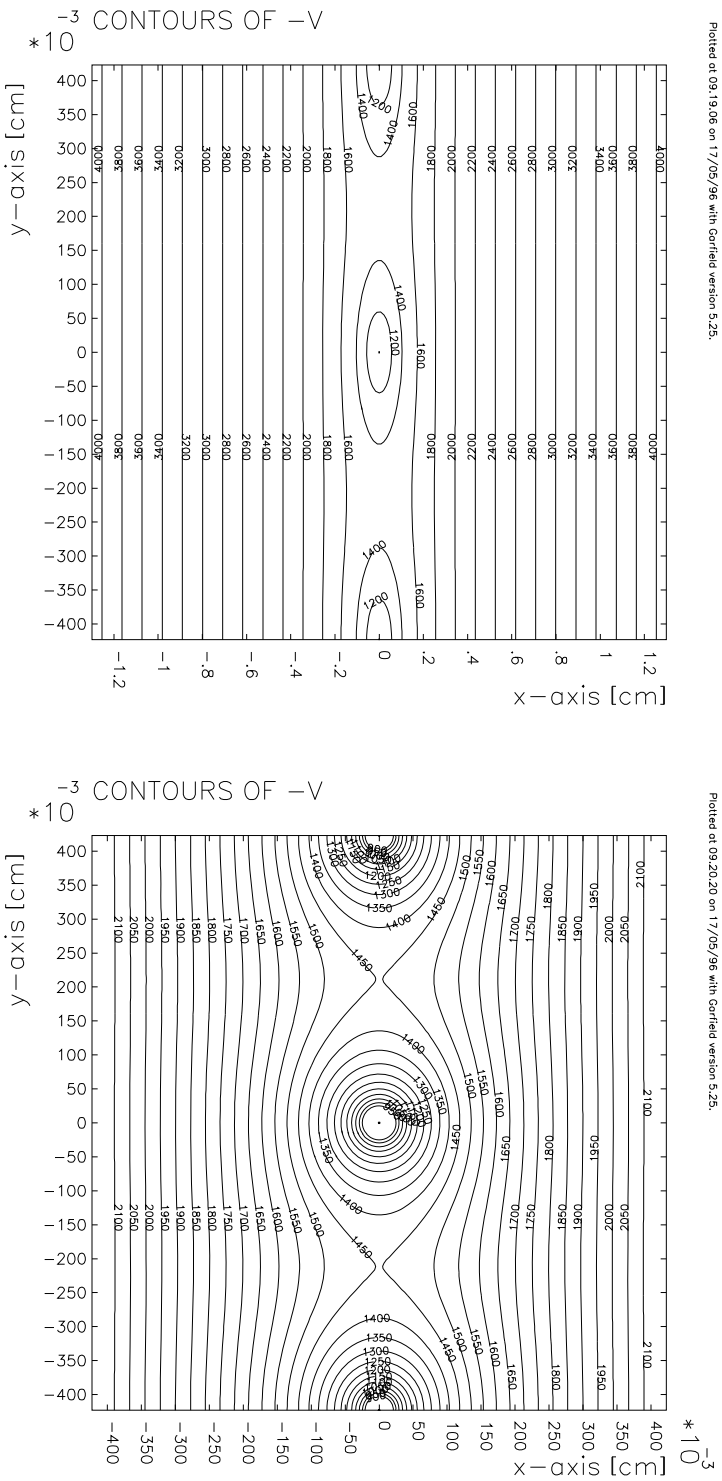

Figure 1-4: The contours of the voltage are shown every 100 V in (a) for the whole width of the chamber and every 50 V in (b) for the region close to the wire. The voltage on the HV planes is -4100V.

creating a signal in several wires. The time that elapses between the primary ionization event and the creation of a signal is roughly proportional to the distance traveled by the drift electron, that is, the distance measured along the field lines from the location of the primary ionization to the wire. By analysis of the distances, perpendicular to the plane of the wires, from the wires to the trajectory of the incident particle for several wires, the angle of the trajectory and the location at which it crossed the wire plane can be determined (Figure 1-5).

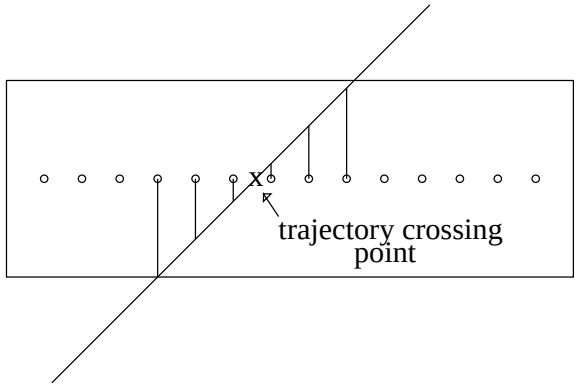

Figure 1-5: The trajectory of the incident particle traverses several wire cells. By determining the perpendicular distances shown, the angle of the trajectory and the trajectory crossing position can be determined.

The length of the path traveled by the drift electron is not the same as this perpendicular distance, however, and an important part of the data analysis in all experiments using drift chambers lies in determining this perpendicular distance from the time measured. It is this problem that I wish to address in my thesis. To do this, I have used a drift-chamber simulation program called `GARFIELD` to simulate the drift-time properties of the chamber.

`GARFIELD` is a computer program written by Rob Veenhof at CERN for detailed simulation of two-dimensional drift chambers [15]. It can be used to calculate field maps, x(t) relations, arrival-time distributions, and signals. It includes an interface to the program `MAGBOLTZ`, written by Steve Biagi, which computes gas properties in arbitrary mixtures of commonly used gases. The program is still under development;

most of the simulations in this thesis were made using version 5.18 (December 1995 release). Input files used to create all GARFIELD-generated plots and data used in this thesis are given in Appendix A.

On the basis of the GARFIELD simulations, algorithms for finding the perpendicular x distance from the trajectory of the incident particle to a wire, given the measured drift time to the wire have been found. The methods presented here have the advantage that they can easily be redone for different chamber parameters, gas mixtures, and voltage settings. This allows predictions about the operation of the VDCs under different conditions to be made, in order to optimize this operation. It also provides a means to avoid analysis of long calibration runs for changes in chamber parameters.

Chapter Two of this thesis discusses in more detail the operation of vertical drift chambers. Chapter Three describes the parameters of the CEBAF Hall A Vertical Drift Chamber and some specifics of its operation, including the drift time distribution. In Chapter Four, the time-domain calculations done by GARFIELD are described. Various methods of parameterizing the simulation results are presented, and the usefulness of these fits for calibration and data analysis at CEBAF is considered. Possible future endeavors with the project are also discussed.

Chapter 2

Theory of Drift Chamber Operation

2.1 Ionization

When a charged particle traverses a gas chamber it transfers energy to the gas, by ionizing molecules and atoms of the gas. The mean rate of ionization loss of a charged particle, as given by the Bethe-Bloch formula [10], is:

$$\frac{dE}{dx} = \frac{4\pi N_o Z^2 e^4}{mv^2}\frac{Z}{A}[\ln(\frac{2mv^2}{I(1-\beta^2)}) - \beta^2]. \tag{2.1}$$

The energy loss to the gas results in the formation of ion pairs (positive ions and negative electrons) in the medium. First the incident particle collides with gas molecules and creates drift electrons, the primary ionization. Those electrons produced in this process that have a high enough energy will create futher inonization themselves; this process is known as secondary ionization. This secondary ionization occurs when the electron has acquired an energy greater than the ionization energy (about 26 eV for Argon).

The Bethe-Bloch formula gives the average value of energy loss dE in a layer of gas dx. There is a Landau distribution about the mean energy loss, which is asymmetric; the tail extends to values much greater than the average energy. This distribution is discussed further in the following section.

2.2 Cluster Size Distribution

One of the factors affecting the space resolution of drift chambers is the non-continuous nature of the distribution of ionization along the particle track, expressed as the cluster-size distribution [6]. As an incident particle traverses the chamber, the ionization of the gas is not a continuous distribution. Instead, this ionization is deposited in lumps, or ionization clusters, each produced as a result of individual primary ionizations. The probability distribution of the number of electrons ionized, either directly or indirectly, by a particle on its trajectory is known as cluster-size distribution. The cluster size, ie, the total number of ions liberated close to the primary ionization event, may vary from one to many electrons, and is roughly proportional to the energy transferred in the primary ionization act (Equation 2.1), and also depends on the ionization energy required to liberate an ion pair. More precisely, it is necessary to determine the spectrum of energy loss $F(E)dE$, and the probability $p(E,k)$ for each energy E of producing exactly k ionization electrons. The cluster size distribution $P(k)$ can then be found by integrating over the energy [3]:

$$P(k) = \int F(E)p(E,k)dE \tag{2.2}$$

Experiments to determine cluster size distribution have been done both experimentally for several gases by Fischle *et al* [6], and for Argon, using computer simulations, by Lapique and Piuz [8], with similar results. The experimental data for Argon are shown in Figure 2-1.

2.3 Drift of Electrons

Once ionization of the gas has occurred, and electrons and ions have been produced, we are interested in the drift properties of these particles. On average, both electrons and ions drift with a constant drift velocity v_D, in the direction of the electric field E. The electron will travel an average distance λ, the mean free path, before it collides with a gas molecule. After an electron collides, it scatters isotropically, due to its small

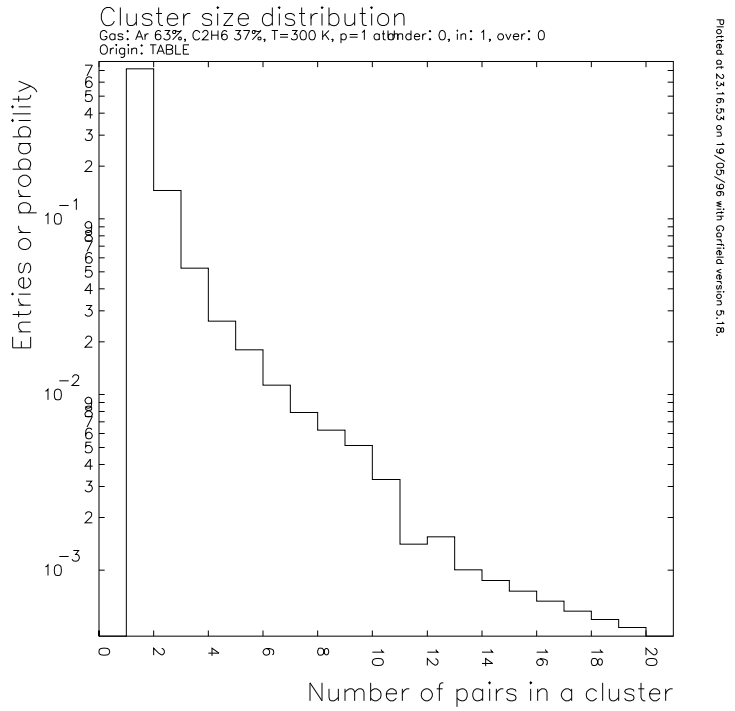

Figure 2-1: The experimentally determined cluster size distribution of Argon [6] is shown, as a function of the number of electron-ion pairs in a cluster. The cluster size distribution is dominated by Argon, and the addition of Ethane or Carbon Dioxide has a very minimal effect [16].

angular momentum. The electron is then accelerated by the field until it collides with another gas molecule. The actual drift velocity is much smaller than the instantaneous velocity between collisions, and is given by:

$$v_D = \mu E = \frac{e}{m} E\tau. \tag{2.3}$$

The scalar mobility μ is defined as the ratio of drift velocity to electric field in the absence of a magnetic field and is proportional to τ, the mean time between collisions [3]. The energy acquired is then transferred, in the next collision, to recoil or excitation. The drift velocity is also affected by the effective fractional energy loss per collision. A full account of these effects is not given here. However, both Sauli [13] and Blum and Rolandi [3] discuss this in further detail. As shown in Figure 1-3, the E field, and thus the drift velocity, is relatively constant for most of the drift distance. Very close

to the wire, however, it increases rapidly, so that the drift velocity becomes very large very close to the wire.

The drift velocity is an important part of the calculation of drift-time properties of the chamber, so it is important that the model used is accurate. In the simulations presented in this thesis, the drift velocity has been calculated by an interface to the `MAGBOLTZ` program for an Argon-Ethane gas mixture. An MIT-LNS group led by Becker has done measurements of drift velocities for several commonly used gas mixtures. These measurements have been compared to the drift velocity provided by Magboltz; the agreement is very good for all measured values, as can be seen in Figure 2-2. The measured values extend to electric field values of 3.2 kV/cm, which accounts for all of the drift area except that within about 1 mm of the wires.

2.4 Drift of Ions

The drift properties of ions differ from those of electrons because they possess a significantly larger mass and interact differently with the gas. This information is not directly used in the simulations that follow, but it is relevant for understanding other aspects of drift chamber operation and a brief discussion is given here. Electrons are more rapidly accelerated in an electric field than ions, and lose very little energy in elastic collisions with gas atoms. In typical drift chambers, electrons reach energies much greater than thermal motions, and their mobility is a function of the energy loss associated with inelastic excitation of gas molecules. [3]

Ions in similar fields acquire a similar amount of energy as do electrons, but much of this energy is lost in the next collision. Additionally, the ion momentum is less randomized in each collision, thus less field energy is stored in random motion, and the random energy of ions is mostly thermal. The result is that the effect of diffusion on ions is orders of magnitude smaller than in electrons. We are interested in the mobility of the ions in a given gas. This mobility is constant up to very high fields, because the average energy of the ions is unchanged, unlike in the case of electrons. Table 2.1 shows the mobility for several ions in argon.

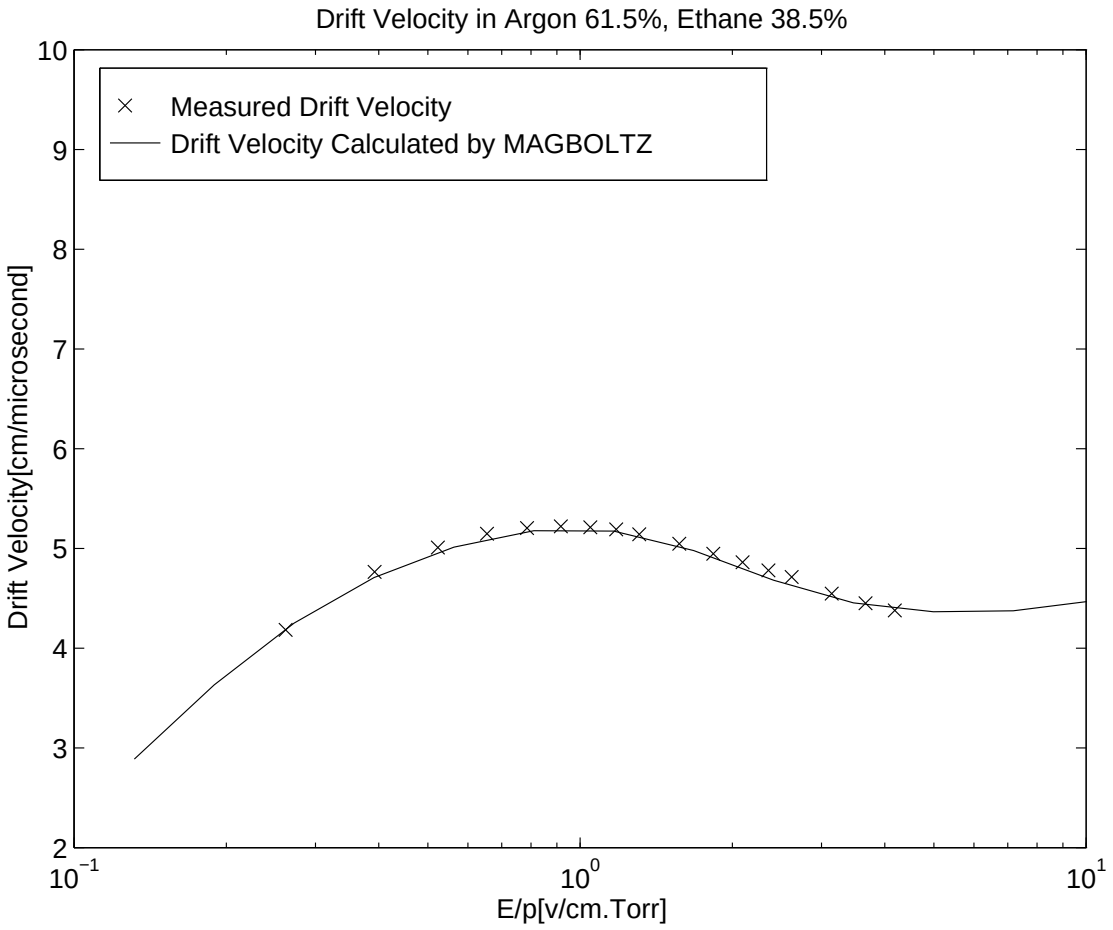

Figure 2-2: The drift velocity calculated by `MAGBOLTZ` is compared with the drift velocity measured by Becker *et al* [1]. Although the measurements do not extend through the entire range of fields in the chamber, they do confirm the validity of the drift velocity for all positions along the drift path but those very close to the wire.

ions	mobility (cm^2/Vs)
$[CH_4]^+$	1.87
$[CO_2]^+$	1.72
$[IsoC_4H_{10}]^+$	1.56
$[Ar]^+$	1.54

Table 2.1: Experimental mobilities of various ions in Argon gas[3]

In a gas mixture, the mobility can be found using Blanc's law:

$$\frac{1}{\mu} = \sum \frac{p_k}{\mu_k}, \tag{2.4}$$

where p_k is the volume concentration of the gas k in the mixture, and μ_k is the mobility of an the ion in the gas k. Blanc's law holds especially for low fields, but is not a bad approximation for higher fields [3].

2.5 Effect of High Electric Fields

A detailed discussion of the field calculations is beyond the scope of this thesis. The model used in the `GARFIELD` simulations, and to produce the plots in Figure 1-3 is discussed in the `GARFIELD` manual [15]. In addition, a more extensive analytical calculation of these equations is carried out by Distler [5].

When drift electrons reach the area of increasing, radial fields, and the field gets above a few keV per cm, an increasing number of them acquire enough energy between collisions to produce secondary ionizations. Ionization may occur whenever the electron gains enough energy to overcome the ionization potential. The average distance an electron must travel before it may collide and produce an ionization is called the mean free path, λ. The inverse of the mean free path for ionization, α, is known as the first Townsend coefficient. Values of the Townsend coefficient for a mixture of Argon-Ethane and a mixture of Argon-Carbon Dioxide are shown in Figures 3-3 and 3-4.

Each collision resulting in ionization liberates another electron-ion pair, which then

in turn can, after traveling the mean free path, liberate more electron-ion pairs, and so on. This creates an avalanche effect near the wire, which serves to amplify the charge produced by the initial ionization of the gas.

Chapter 3

The CEBAF Hall A VDC

3.1 Chamber Specifications

CEBAF Hall A contains two high resolution spectrometers. Each spectrometer has two VDCs aligned at a 45-degree angle to the track of the particles, and in the focal plane of the spectrometer (see Figure 1-1). Each VDC has two orthogonal wire planes, which consist of 400 parallel sense wires held at ground potential, and oriented 45 degrees with respect to the chamber (see Figure 3-2). These are positioned between high-voltage planes made of gold-coated mylar. On the outside of the HV planes there are gas containment windows made of aluminized mylar. These VDCs are unusual in that they do not include guard wires, often included to help shape the field [12]. The exclusion of these allows for reduced chamber thickness, and reduced multiple scatterings for the same field strength. Figure 3-1 shows the details of the chamber parameters. A more complete discussion of the construction of the VDCs is given by Leathers [9].

The field is nearly constant throughout the chamber, except near the sense wires, where it becomes very strong (Figure 1-3). These wires are very thin; 20μm, and the strong field they establish creates an avalanche near the wire, which amplifies the signal. The orientation of the chamber is such that an incident particle will in general create a signal in several wires in each VDC (Figure 1-5). Thus manipulation of the drift times measured for these wires gives an accurate determination of the path of

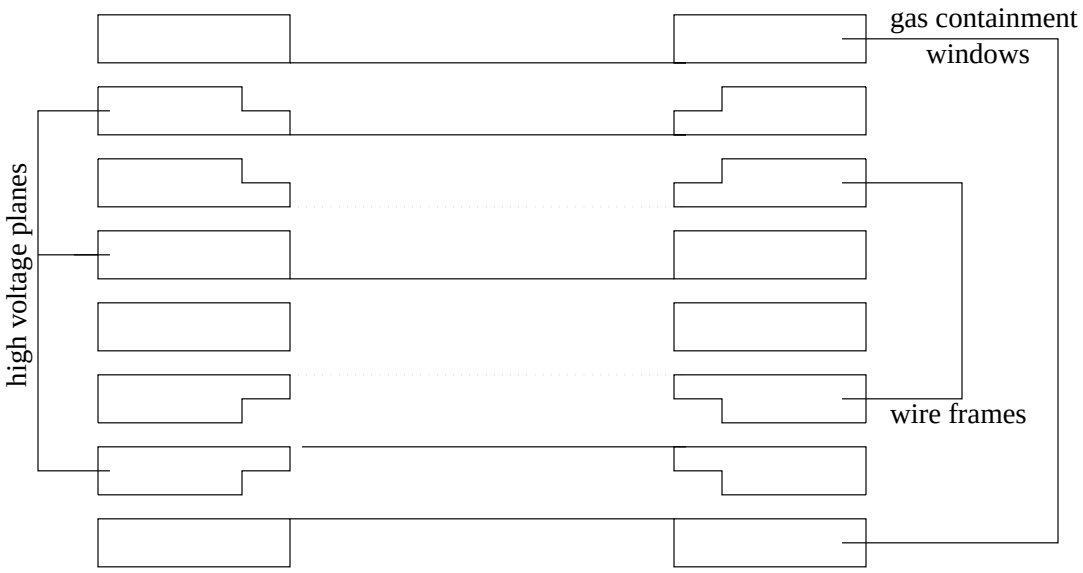

Figure 3-1: The details of construction of the Hall A VDC are shown. The gas containment windows are made of aluminized mylar. The high voltage planes are gold-plated mylar; the middle plane is coated on each side, the outside planes are gold-plated on the inside only.

the particle; both its angle through the VDCs and the position at which the trajectory crosses the wire plane. The setup can achieve a position accuracy of 100 μm [4].

All calculations that follow can easily be repeated for changes in chamber parameters, voltage settings, or gas mixtures, by varying the appropriate parameter in `GARFIELD`.

3.2 The Angle of the Trajectory

The spectrometer preferentially selects trajectories by momentum, and thus only trajectories within a certain angle range will traverse the chamber. This angle range is approximately 38 to 52 degrees, with respect to the plane of the chamber (the y-z plane in Figure 3-2). It turns out that it is most convenient, for purposes of simulations using `GARFIELD` and for developing a reconstruction parameterization, to define the

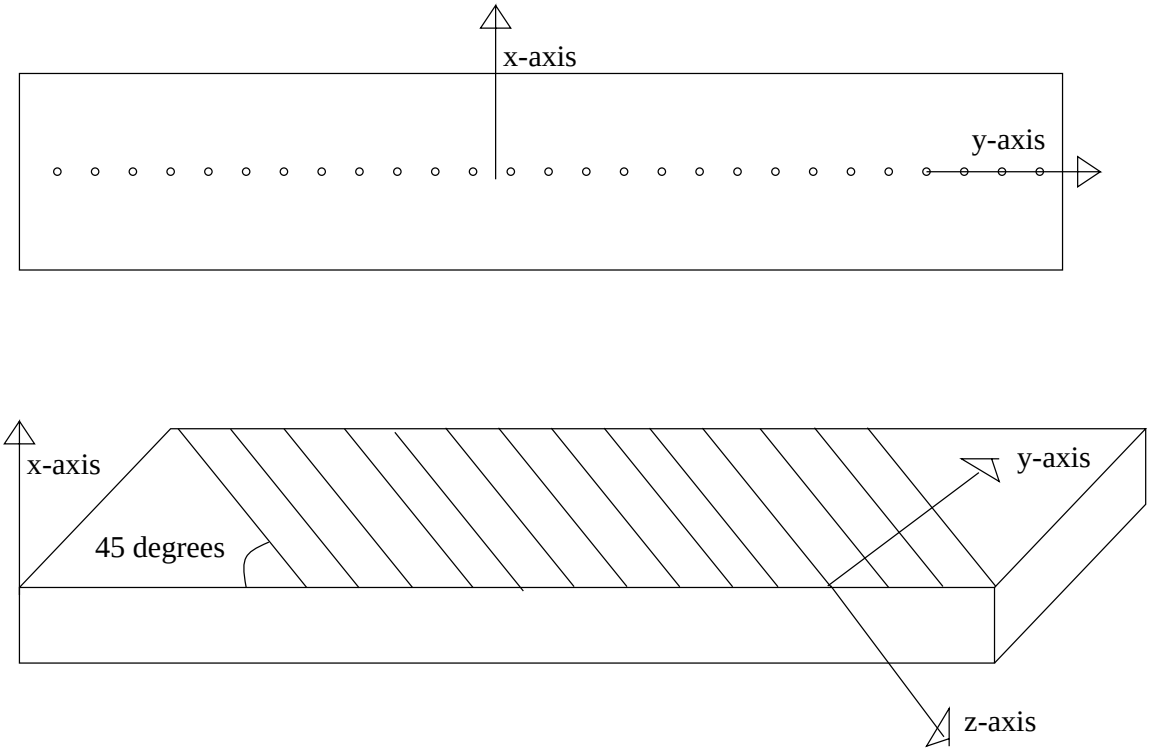

Figure 3-2: The coordinate systems of the wire planes is shown. The top picture is an edge-on view, in which the z-axis, along the wires, is defined perpendicular to the page. The second figures shows the inclination of the wires with respect to the frame. The wires in the other wire plane are oriented so that they are orthogonal to the ones displayed.

angle differently. `GARFIELD` is essentially a two-dimensional program, and cannot account for the orientation of the wires with respect to the chamber. Thus for the rest of this thesis, the angle used will be θ', which is defined as the angle that the projection of the incident trajectory onto the x-y plane, in the coordinate system shown above, makes with the y-axis. Note that the y-axis in this coordinate system is not parallel to the frame of the chamber, instead it is perpendicular to the orientation of the wires. From simple geometric arguments, for an incident trajectory of θ, this angle is given by

$$\theta' = \arctan[\tan\theta / \cos\phi], \tag{3.1}$$

where ϕ is the angle of the wires with respect to frame of the chamber, equal to 45 degrees. The corrected angle of the trajectory, θ', will then fall approximately within the range of 46 to 62 degrees. It is this angle range that will be explored in subsequent sections.

3.3 Calculation of Gas Characteristics

The original choice of gas for the VDCs was a mixture of 62.9% Argon and 37.1 % Ethane, and most of the calculations in this thesis were done using this gas mixture. There were concerns about the safety of this gas mixture at CEBAF, however, and they have now switched to a mixture consisting of 85% Argon and 15% Carbon Dioxide. Applications to this change in gas mixture will be discussed where possible.

The properties of the ionizing gas used to fill the chamber are calculated using an interface from `GARFIELD` to the `MAGBOLTZ` program. The program calculates drift velocity, Townsend coefficients, diffusion coefficients, and attachment coefficients. These calculations are shown for each of the gases mentioned above. The diffusion coefficient is a measure of how much drift velocity deviates from the mean due to random variation; the attachment coefficient measures the capability of gas molecules to absorb drift electrons. A more detailed discussion of these parameters is given in [3].

3.4 Drift Lines

Figure 3-5 shows drift-lines and equal-arrival-time contours for minimum and maximum angles through the chamber. The drift lines are the lines on which drift electrons travel, under the influence of an electric field, after they have been ionized. An electron drifting on any drift line, starting at some position on a contour of equal arrival-time, will reach the wire at the same time.

The drift lines are often modeled as being constant and perpendicular to the wire plane until some specific time, and, for smaller times, as extending radially from the wire. These drift line plots show that this model may be lacking in accuracy; instead of

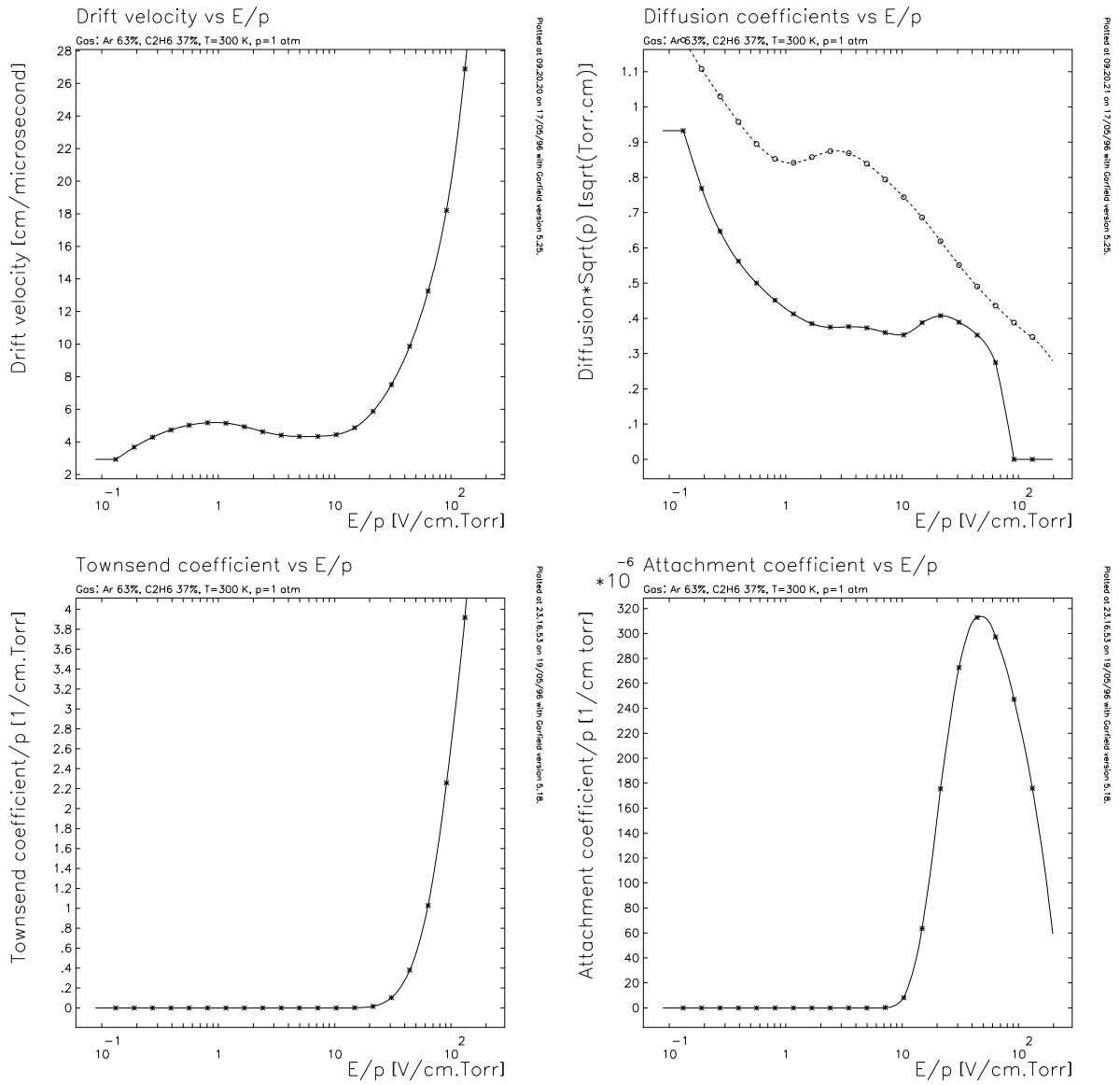

Figure 3-3: Drift velocity, transverse (dashed line) and longitudinal (solid line) diffusion coefficients, the Townsend coefficient, and the attachment coefficient are shown, as calculated by the `GARFIELD` interface to `MAGBOLTZ`, for a mixture of 62.9% Argon and 37.1% Ethane. This is the mixture used for the algorithms discussed in Chapter 4.

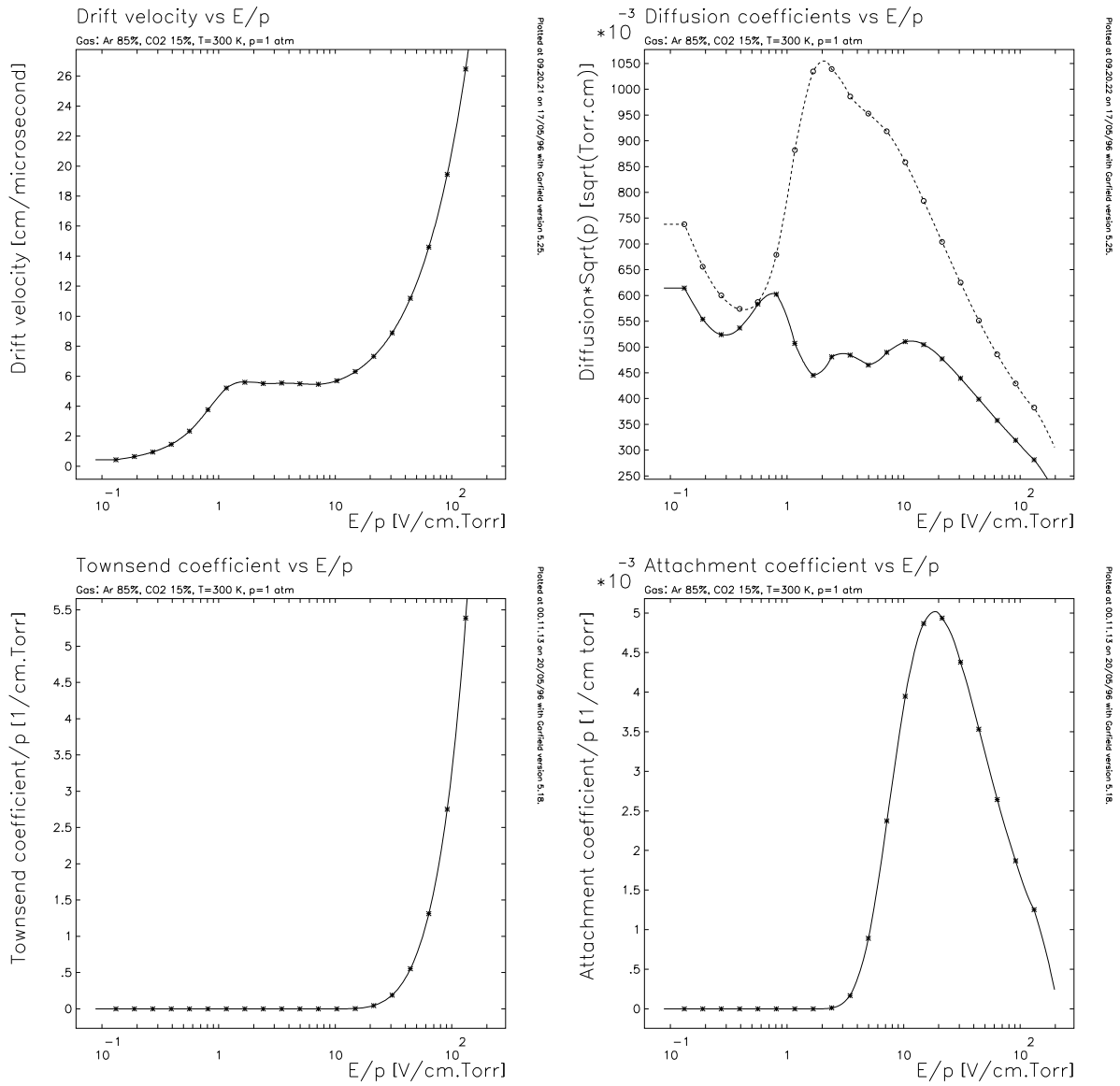

Figure 3-4: Drift velocity, transverse (dashed line) and longitudinal (solid line) diffusion coefficients, the Townsend coefficient, and the attachment coefficient are shown, as calculated by the `GARFIELD` interface to `MAGBOLTZ`, for a mixture of 85.0% Argon and 15.0% Carbon Dioxide, the mixture currently being used in the CEBAF Hall A VDCs.

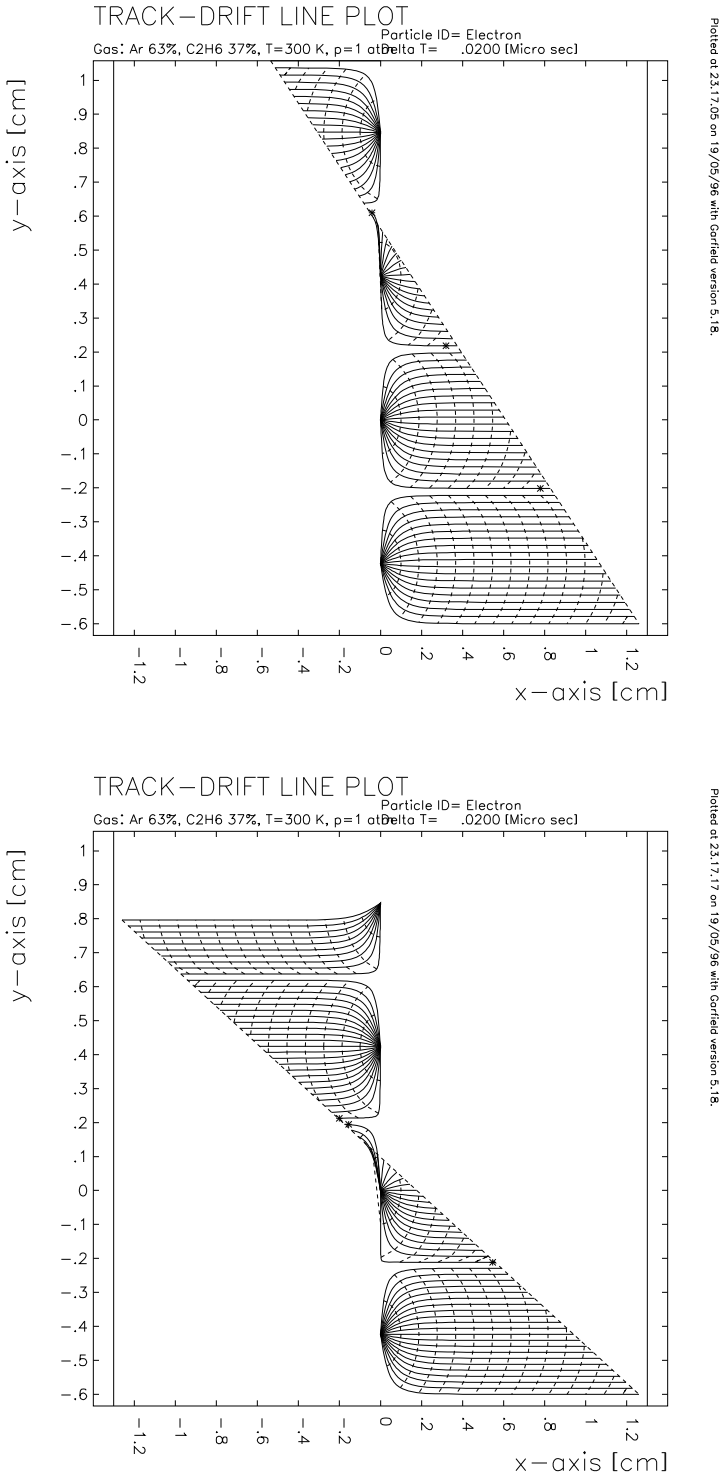

Figure 3-5: Drift lines are shown for two different track angles. The angles shown are the minimum and maximum trajectory angles, which are each 7.5 degrees away from the mean. This mean, which is a 45 degree incident trajectory, corresponds to an angle of 54.74 degrees. Contours of equal arrival time are marked every 20 ns.

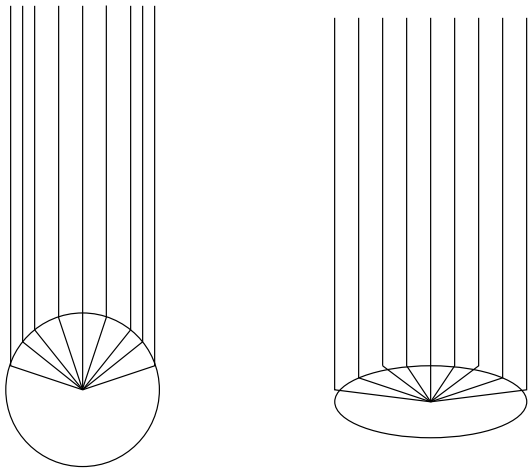

Figure 3-6: Figure (a) shows an approximation in which the field lines make a transition to a radial field at one specific radius. Figure (b), which corresponds much better to the drift lines as modeled by GARFIELD, approximates this transition as an angle-dependent ellipse.

this transition occurring at a circle of constant radius, it occurs at an angle-dependent ellipse (Figure 3-6).

3.5 Distribution of Arrival Times

Figure 3-7 shows the drift-time spectrum for Argon-Ethane. Figure 3-8 shows the same distribution for an Argon-Carbon Dioxide mixture, both as it was calculated by GARFIELD, and as measured with the actual apparatus at CEBAF. The central, plateau region of the spectrum corresponds to a constant drift velocity. This distribution is flat in the region of constant drift velocity if the chamber is uniformly illuminated with particles. For large times, a maximum drift distance is reached, and spectrum quickly falls to zero. For shorter times, there is a peak in the spectrum. This increase is primarily due to the nature of the curved field-lines closer to the wire, which result in more events where the drift time is shorter.

This can be seen by noting that the number of counts in an interval of the drift-time spectrum is given by

$$\frac{dN}{dt} = \frac{dN}{ds}\frac{ds}{dt}, \tag{3.2}$$

where s is the length of the path traveled by the drift electron. The drift velocity, ds/dt, is essentially constant, except very close to the wire. dN/ds is the effective flux through the drift line. In the parallel-plate field region, where the drift is perpendicular to wires, this is equal to the flux Φ times $\cos\alpha$, where α is the track angle, the angle of the trajectory with respect to a perpendicular to the drift lines. The angle α is equivalent to the angle θ' in this linear field region. The flux Φ is just the number of tracks per cm through a line perpendicular to the trajectory, and is constant. In the approximation of Figure 3-6 (a), once a drift electron has entered the radial region, the shortest drift line is perpendicular to the track, and thus the effective flux through the drift line is equal to Φ. This results in an increase in dN/ds, and causes the peak seen in the spectrum at small times. There is a very sharp peak in the region very close to the wire; here the drift velocity is increasing rapidly and the drift time can become quite short.

A traditional method of drift position calibration uses this distribution to convert drift times to track-crossing distances. The chamber is illuminated with a "white" particle spectrum. This illumination is uniform with track-crossing distance and angle, and produces a spectrum like that seen in Figures 3-7 and 3-8 . The number of counts in an interval of the drift-time spectrum can also be given by

$$\frac{dN}{dt} = \frac{dN}{dx}\frac{dx}{dt} = \Phi * \frac{dx}{dt}. \tag{3.3}$$

For each time interval dt, dN/dt is the number of counts in that interval, and dN/dx is the flux Φ, a constant number of counts per unit x_{perp}. The drift velocity, as discussed, is constant through most of the region, but increases rapidly for very short times. The effective drift velocity, ie, the drift velocity along the x-axis, is given by

$$\frac{dx}{dt} = \frac{1}{\Phi}\frac{dN}{dt}. \tag{3.4}$$

This can be integrated to find the corresponding perpendicular distance:

$$x(t) = \int_0^t \frac{1}{\Phi}\frac{dN}{dt'}dt', \tag{3.5}$$

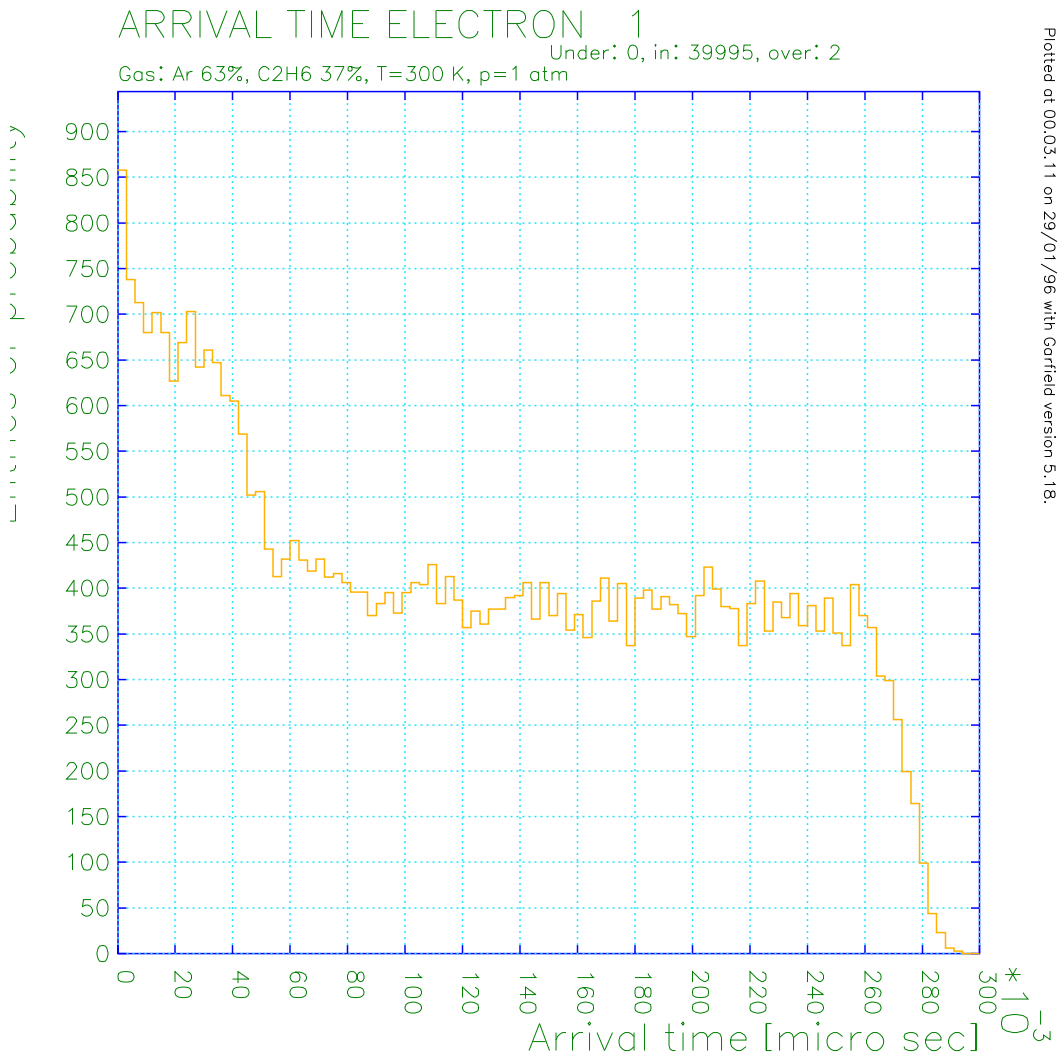

Figure 3-7: Distribution of the arrival time of drift electrons in an Argon-Ethane gas mixture, is shown as calculated by `GARFIELD`, for a spectrum that ranges over track angle and track crossing position.

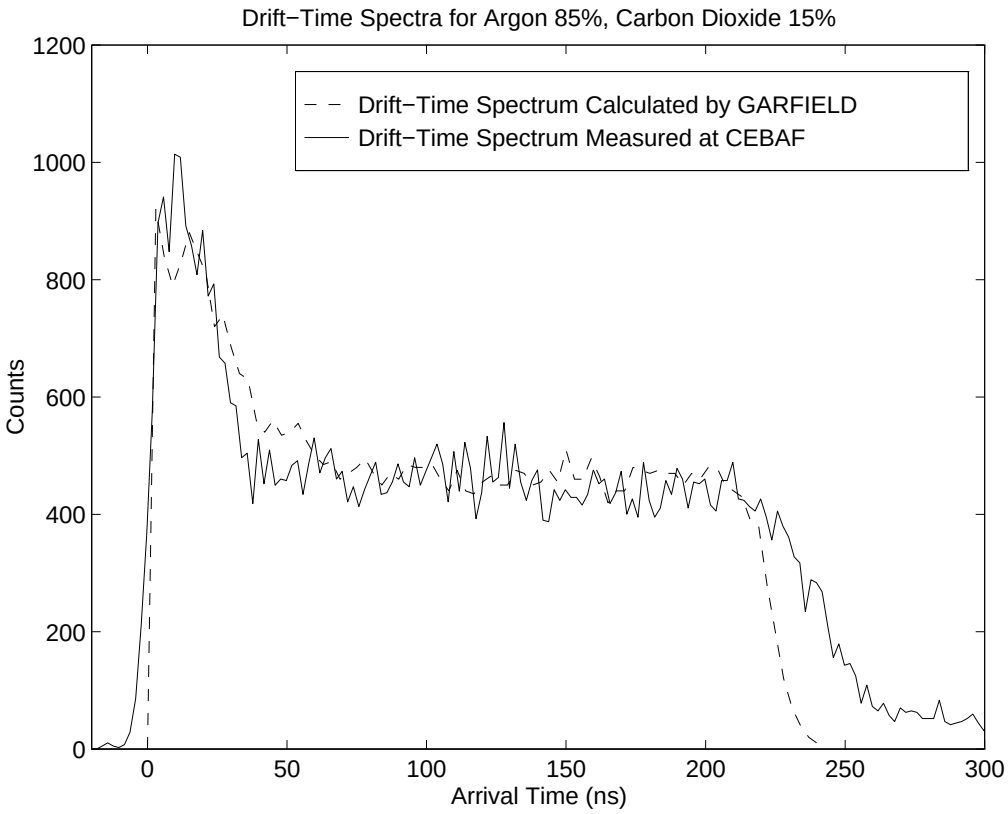

Figure 3-8: Distribution of the arrival time of drift electrons for an Argon-Carbon Dioxide gas mixture is shown, as calculated by `GARFIELD`, and as measured at CEBAF. The only discrepancy is in the falloff, which is probably due to a wider angle range used at CEBAF. This wider angle range can account for longer maximum drift times.

where the flux can be found by requiring that $x(t_{max}) = x_{max}$ [14].

This method has the great disadvantage that it requires a lengthy calibration run to be done for any change in chamber parameters, gases, or data acquisition techniques. Other methods have been tried, see especially the theses of Jordan [7] and of Distler [5]. The next chapter will explore other methods of doing this drift time to drift distance calibration.

Chapter 4

Methods for Drift Time Calibration

4.1 Time-Domain Response in GARFIELD

We are interested in calculating the relation between minimum drift time to the wire and the perpendicular x-distance from the trajectory to the wire. GARFIELD provides two alternate ways to do this calculation; one using the *xt-plot* instruction, and the other using the *arrival-time* instruction.

The instruction *xt-plot* functions by minimizing the drift time over a series of parallel lines, that is, parallel tracks through the chamber at the user-specified angle, for a series of starting points. First drift lines are calculated for each of the tracks. The perpendicular drift distances are found for each of the three drift lines with shortest drift times to the wire. This is desired because the ionization event which results in a signal in the wire will be the one that has the minimum drift time, and is the first to drift to the avalanche region. If the three smallest drift times are not consistent, within the range of a user-specified accuracy parameter ϵ, the minimum drift time is recalculated. The three smallest times are then replaced with this new minimum plus or minus a small value. This process continues until the desired accuracy is reached. It does not take clustering effects into account, but does give information about the diffusion to be expected on the drift line that gives the smallest drift time.

The internal accuracy of this method maybe as good as 0.1%, but Veenhof points out that this may be inaccurate because of uncertainties in the drift velocity, and

perhaps should not be used as a direct input to a reconstruction program without corrections [15]. We have shown, however, that the drift velocity used in the simulations is very consistent with experimental data.

The *arrival* instruction operates on the same tracks as *xt*, but takes more information into consideration in its computations, including the cluster-size distribution, and the attachment and diffusion coefficients. For each track, the instruction generates clusters a specified number of times, computes the drift-time and generates integrated diffusion coefficients for each electron of each cluster. The *arrival* method is a Monte-Carlo computation, thus it is costly in terms of computation time and may have less internal consistency than *xt*. Since it takes more of the gas characteristics into effect, however, *arrival*'s computations are usually closer to what is actually measured.

Figure 4-1 compares results of the two methods for three different incident angles. The methods presented in Section 4.2 use the *xt* calculations because of the gain in computation time; the data used is shown in Figure 4-2. No significant alterations would be required to use the *arrival* numbers in either method discussed in the following sections.

4.2 Fitting the Simulation Data for Calibration and Analysis

In this section, two algorithms will be discussed for converting the measured drift time to the x-coordinate of the trajectory with respect to the wire. This information, when found for several wires for one event, can be used to determine the angle of the trajectory and the trajectory crossing point. The first involves introducing and parameterizing a correction function that relates the actual distance traveled to the x-coordinate desired. The second involves an interpolation directly from `GARFIELD` data.

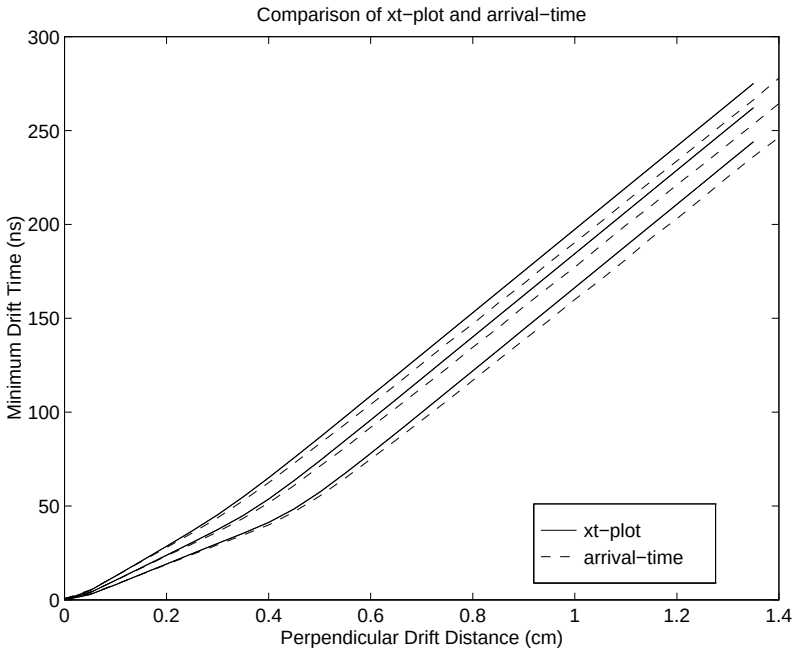

Figure 4-1: The results of the `GARFIELD` instructions *xt-plot* and *arrival-time* are shown for three different incident angles.

4.2.1 Parameterization of the Correction Function

The x coordinate of interest for further analysis of the data is not the length of the actual path traveled by the drifting electron; we are interested in the distance of the path from the wire on a line intersecting the wire and perpendicular to the wire plane. In figure 4-3 it can be seen that the particle will travel on the field line with the shortest drift time, and that this drift distance is shorter than the x coordinate distance of interest, x_{perp}.

The actual drift distance traveled, given a drift electron that was found to have a drift time t_{meas} and is assumed to be traveling at a constant drift velocity v_D is

$$x_{min} = v_D t_{meas}. \tag{4.1}$$

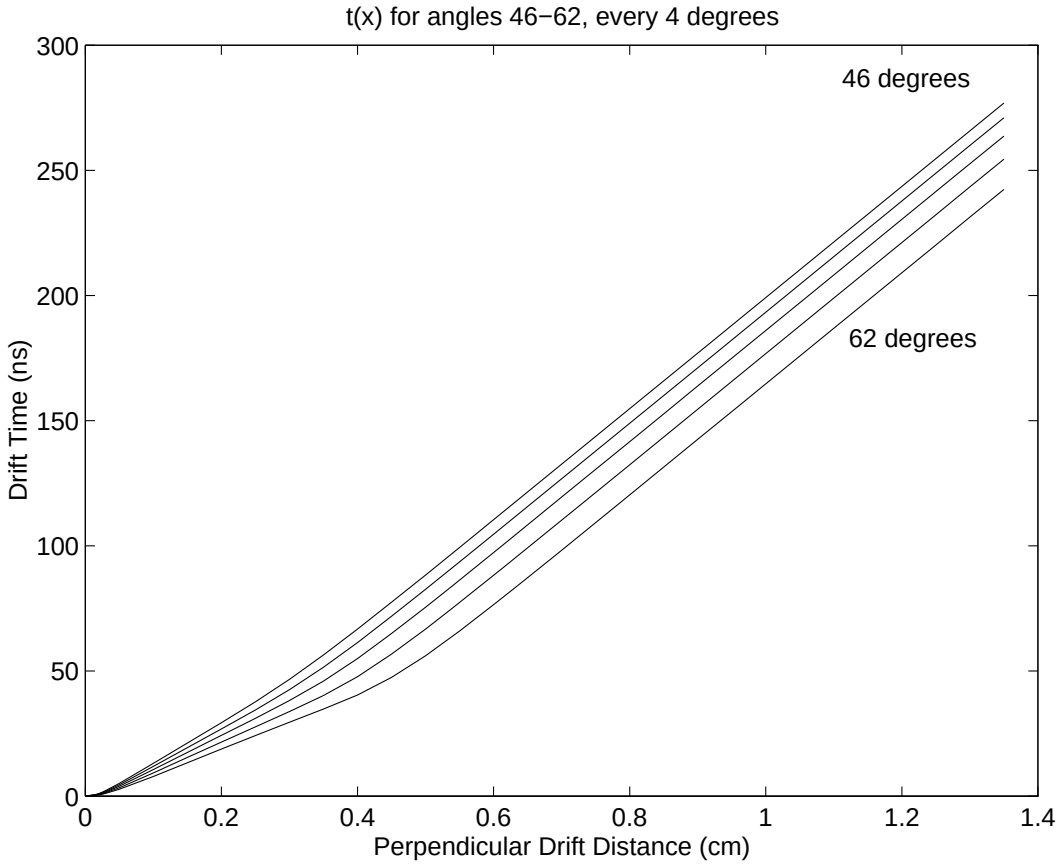

Figure 4-2: The minimum drift time, as a function of perpendicular distance to the wire, is shown for several different track angles, as calculated by the *xt-plot* instruction. This is the data used in the parameterizations that follow.

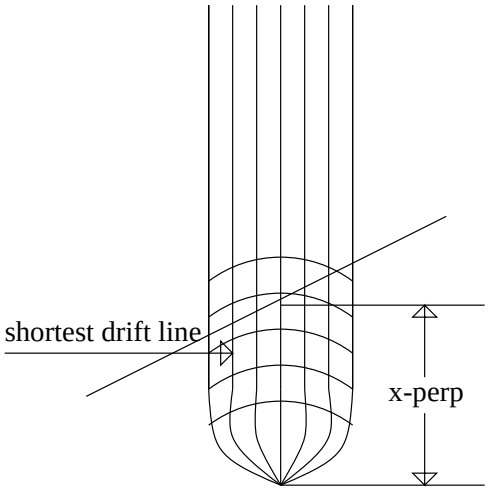

Figure 4-3: Drift lines for one wire cell. The curved lines are lines of equal drift time. Aslo shown are the actual path the drift electron takes (on the drift line with corresponding to the shortest drift time), and the perpendicular distance, x_{perp}.

The distance must then be corrected by some distance x_{corr}, so that

$$x_{perp} = v_D t_{meas} + x_{corr}. \tag{4.2}$$

This correction factor can be found using data from `GARFIELD` simulations:

$$x_{corr} = x_g - v_D t_g, \tag{4.3}$$

where t_g is the time calculated by `GARFIELD` for a given perpendicular distance x_g.

Figure 4-4 shows this correction function, as a function of the drift time, for several angles. For a specific angle θ, the correction increases with drift time until a certain t_o, at which point it becomes constant. For drift times larger than this t_o, the drift velocity is approximately constant, and the field lines are straight and perpendicular to the wire plane. The correction factor x_{corr} is thus a constant function of θ, $x_c(\theta)$.

As the particle approaches the wire, the field lines become approximately radial and the electron no longer drifts perpendicular to the wire. For all but very small t, we can then approximate the correction function by a line whose slope is dependent on x_c and t_o. For very small t ($t \leq 1.2$ ns), the drift velocity increases very rapidly, and there is no longer a purely linear relation between position and time. The correction for these

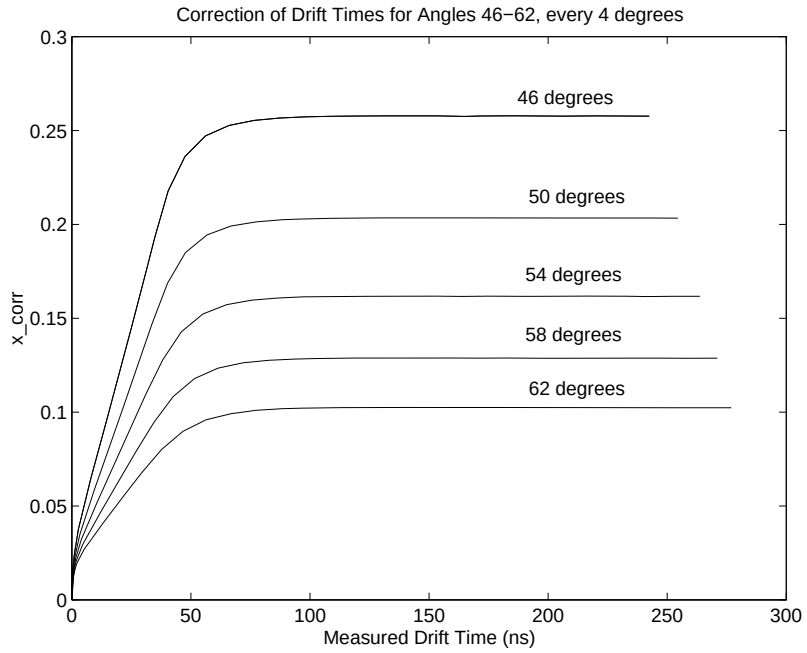

Figure 4-4: The correction to the drift distance x_{min}, defined as $x_g - v_D t_g$ is plotted with respect to the measured drift time t, for angles from 46 to 62 degrees, every four degrees.

times diverges from this line in the radial drift region, but is not strongly dependent on θ. It is most useful, then, to approximate this by one short line, independent of the angle of the trajectory.

The correction function is then as follows:

$$x_{corr} = x_c(\theta) \text{ for } t_{meas} \geq t_o(\theta) \tag{4.4}$$

$$x_{corr} = \frac{x_c - \Delta x}{t_o - \Delta t} t_{meas} + \Delta x \text{ for } t_{meas} \leq t_o(\theta) \tag{4.5}$$

$$x_{corr} = \frac{\Delta x}{\Delta t} t_{meas} \text{ for } t_{meas} \leq \Delta t \tag{4.6}$$

This fit is shown in 4-5. Here, $\Delta x = .195$ mm and $\Delta t = 1.2$ ns. It becomes significantly less accurate when the drift time is in the range 0.04 μs$\leq t_{meas} \leq$ 0.06 μs, and this lack of accuracy increases with increasing θ. For an angle of 46 degrees,

it is at most off by about 60 μm; at an angle of 62 degrees, it can differ by as much as 200 μm. For this reason, it is recommended that another method be used for large angles, or if more accuracy is necessary than this method can provide.

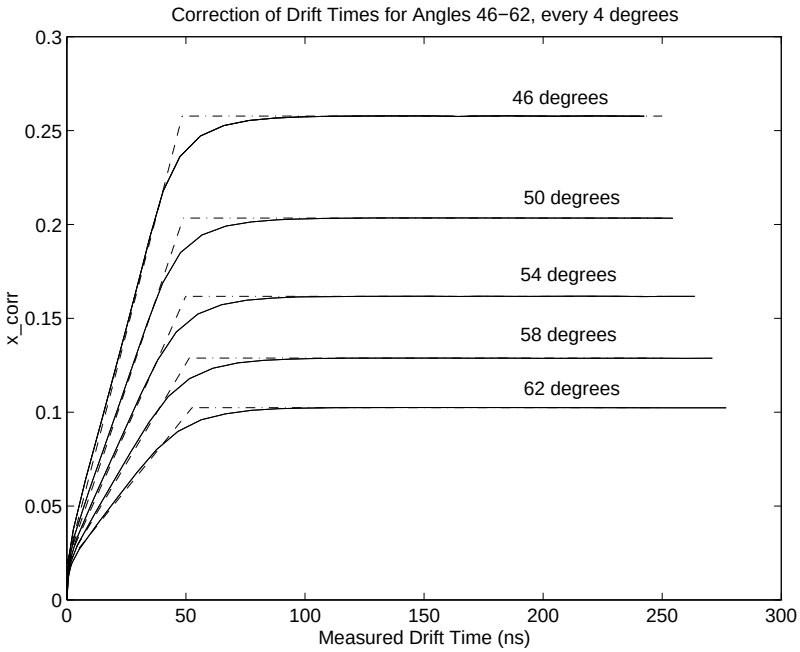

Figure 4-5: Correction to the shortest drift distance. This correction may be approximated by three straight lines, as described in equations 4.4, 4.5, and 4.6. The error is greatest for very small times and for times close to the parameter t_o; for a path of 54 degrees an error of as much as 50-125 μm may occurs between 30 ns$\leq t \leq$45 ns.

The two fit parameters, x_c and t_o are shown in the Figure 4-6 as functions of the angle θ. Each must be fit with a polynomial. The parameters of these polynomials are given in the figure.

4.2.2 Bilinear Interpolation from a Table of GARFIELD Data

In cases where the above method is insufficiently accurate, or in the case that one is interested in a determination of the effects of a change in chamber gases or chamber parameters, without a redetermination of the parameters necessary for the algorithm above, the method of bilinear interpolation from a table of data may be very useful.

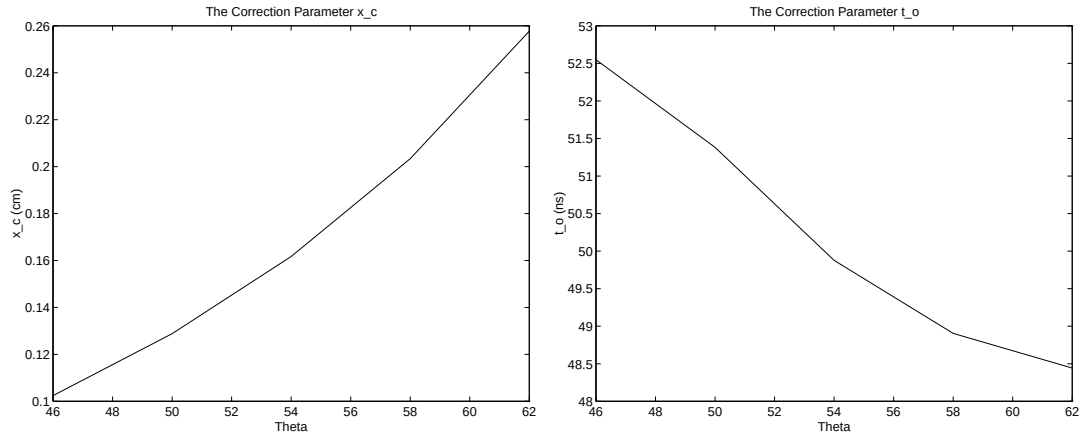

Figure 4-6: The correction parameters x_c and t_o are shown as functions of the angle θ. A second order polynomial is used to fit x_c: $x_c = 0.0003\theta^2 - 0.0216\theta + 0.4836$, while t_o is fit with a third order polynomial: $t_o = 0.0011\theta^3 - 0.1698\theta^2 + 8.3713\theta - 80.5184$.

In order to make use of this method to determine x position from measured drift times, it is necessary to construct a table of values consisting of the positions corresponding to several angles and drift times. I have done this for angles ranging from 46 to 62 degrees and drift times ranging from 0.0 μs to .25 μs for the chamber parameters discussed. This data can also be quickly calculated from `GARFIELD` for different parameters.

The basic method of bilinear interpolation on a table of values is discussed in *Numerical Recipes* [11]. The method is as follows: first, a grid of the four tabulated x values surrounding the desired value is found. If we seek the x for a given t_1 and θ_1, we first find j and k such that

$$t[j] \leq t_1 \leq t[j+1] \tag{4.7}$$

$$\theta[k] \leq \theta_1 \leq \theta[k+1]. \tag{4.8}$$

This is done using a bisection algorithm which will locate the right value in about $\log_2 n$ tries, where n is the number of data points in the table $xdata$. The four points surrounding the desired value are then given by:

$$x_1 = xdata[j][k] \tag{4.9}$$

$$x_2 = xdata[j+1][k] \tag{4.10}$$

$$x_3 = xdata[j+1][k+1] \tag{4.11}$$

$$x_4 = xdata[j][k+1]. \tag{4.12}$$

The simplest way to interpolate in two dimensions is then to define

$$u \equiv \frac{(t_1 - t[j])}{t[j+1] - t[j]} \tag{4.13}$$

$$v \equiv \frac{(\theta_1 - \theta[k])}{\theta[k+1] - \theta[k]}. \tag{4.14}$$

We then approximate that

$$x(t_1, \theta_1) = (1-u)(1-v)x_1 + u(1-v)x_2 + uvx_3 + (1-u)vx_4 \tag{4.15}$$

.

This method results in a very smooth function x(t), that is always between the values given in the table, and varies continuously between grid squares. It compares exceptionally well with the input data; Figure 4-7 compares x-t information from Garfield for 51 degrees with the values found by interpolation. A more accurate method, that of interpolating a polynomial of order 3 or 4 using the 3 or 4 values in each dimension in the table that are closest to the desired value can also be used, but much calculation time is lost and this sort of accuracy is probably not necessary. Both of these methods are discussed further in Appendix B.

Depending on how much accuracy is desired, then, and how important speed of computation is, bilinear interpolation can be a useful alternative to the first method

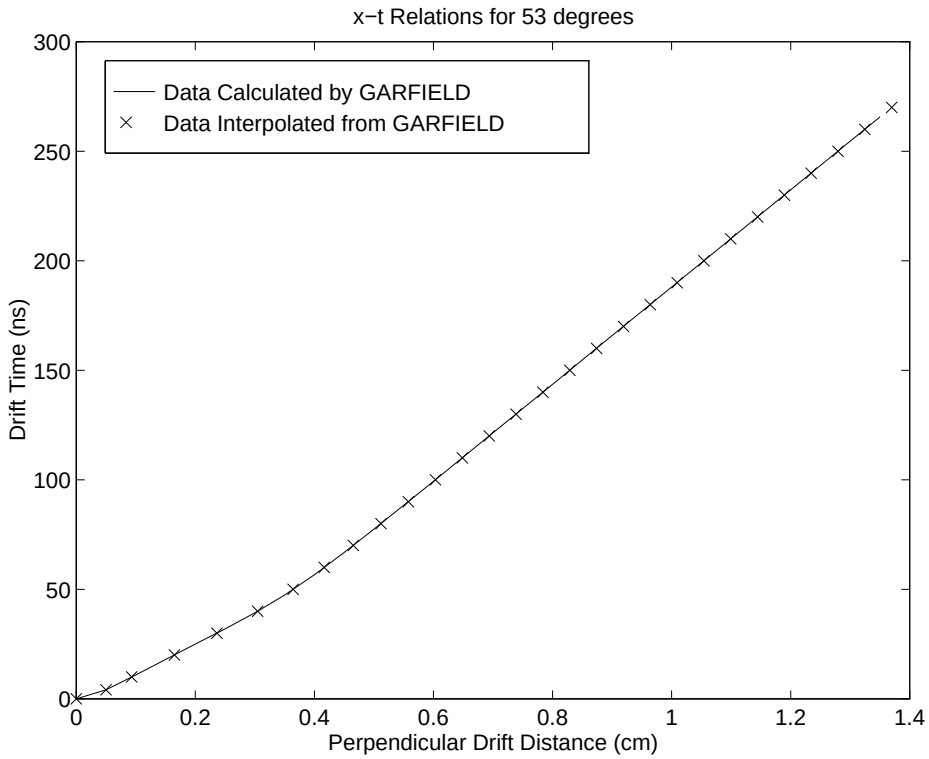

Figure 4-7: The x-t relation for a 53 degree trajectory, as calculated by Garfield, is compared to the same relation as found by interpolation from the table given in B.1.1. The results are accurate to within the accuracy possible with the CEBAF VDC's.

described. None of the problems with very divergent values of the correction for certain values of t arise. I found this algorithm to be fairly efficient; with a table of 32 x values and 9 θ values, it takes about 240 microseconds per event when written in C and run on a SPARC5. In addition, the data used in the table is very easy to get using `GARFIELD`, and may be quickly recalculated in chamber parameters or gas mixtures are changed. If the *xt* instruction is used, the information for all angles is calculated in one or two minutes, if *arrival* is used, it takes an hour or two. `GARFIELD` calculates a table of t values for fixed x's, however, this method requires a table of x values for fixed t's. This table is generated from the `GARFIELD` table by using the above interpolation method in reverse.

4.3 Conclusion

The problem of finding an efficient and accurate method to reconstruct perpendicular drift distances from measured drift times remains an important one in experiments using vertical drift chambers. The methods presented above may be very useful in drift-time to drift-distance calibration at CEBAF, and with slight modification could easily be used with other drift chambers. If small angles are being studied, the first method may be accurate enough. Overall, the method of bilinear interpolation is recommended if 100 μm accuracy is desired. This method corresponds to the input data to well within this range, but the accuracy of the actual input data generated by GARFIELD still needs to be assessed. This method is quick and requires almost no extra work to change the values of the input data to accommodate changes in chamber parameters. With further study, more efficient methods may be found that are based on one of the algorithms discussed.

Appendix A

GARFIELD input

All GARFIELD input files used in making plots and data for Chapter Three are presented in this appendix.

A.1 The Cell

The write command in the following file, and the similar command in the gas section that follows, allow GARFIELD to do the calculations once and write them to datasets. These datasets can then be quickly recalled in subsequent runs without additional calculation, as shown in the field and drift sections.

```
& CELL
opt cell-pr
plane x=-1.3  v=-4100
plane x=+1.3  v=-4100
rows
S 41 .002  0.0 -8.46+(0.423*I)

write dataset vdc

& QUIT
```

A.2 Gas Parameters

As dicussed in Chapter 3, cluster data must be explicitly supplied to the program; all other gas characteristics are calculated by an interface to `MAGBOLTZ`. This file generates Figure 3-3.

```
& GAS
opt gas-plot
magboltz argon 0.629 ethane 0.371
parameter mean 31
cluster
0 69.67 14.13 5.1 2.55 1.75 1.1 0.77 0.61 0.5 0.32 0.137
0.151 0.098 0.085 0.074 0.065 0.057 0.051 0.046 0.041

write dataset argeth 63-37

& QUIT
```

A.3 Electric Field

The following file generates Figures 1-3 and 1-4:

```
& CELL
get vdc

& FIELD
area * -1.0 * 1.0
track -1.3 0.0 -0.01 0.0
plot graph sqrt(EX**2+EY**2)
track * * -0.3 *
plot graph sqrt(EX**2+EY**2)
track -0.3 * -0.05 *
plot graph sqrt(EX**2+EY**2)
track -0.05 * -0.0001 *
plot graph sqrt(EX**2+EY**2)
```

```
grid 25
area * -.423 * .423
plot cont -v  range 1200 4000 n=14
area -0.423 * 0.423 *
plot cont -v range 900 2100 n=24

& QUIT
```

A.4 Drift Properties

A.4.1 DRIFT

The following file generates figure 3-5:

```
& CELL
get vdc

& GAS
get argeth

& DRIFT
EPS 1.0E-07
area  -1.4 -0.6345  1.4 1.0575
lines 80
drift wire l-pr contour 0.2

* min-angle track

track -1.26 1.727 1.26 -0.6
drift track time-graph contour 0.020

* max-angle track

track -1.26 0.796 1.26 -0.6
drift track time-graph contour 0.020

& QUIT
```

A.4.2 X-T PLOT

The following file will store its calculations in a dataset called xt.dat, and will plot xt relations for each specified angle. These plots are not shown individually in this thesis, but the data from them is displayed in Figure 4-2. These data are also used to generate the table given in Section B.1.1.

```
& CELL
get vdc

& GAS
get argeth

& DRIFT
area  -1.5 -0.3  1.5 0.3
select 21
lines 100

*46.0
xt-plot angle 46.0 x-range 0.0 1.40 x-step 0.05 plot-xt-relation ...
  print-xt-relation dataset xt.dat 46deg
*48.0
xt-plot angle 48.0 x-range 0.0 1.40 x-step 0.05 plot-xt-relation ...
  print-xt-relation dataset xt.dat 48deg
*50.0
xt-plot angle 50.0 x-range 0.0 1.40 x-step 0.05 plot-xt-relation ...
  print-xt-relation dataset xt.dat 50deg
*52.0
xt-plot angle 52.0 x-range 0.0 1.40 x-step 0.05 plot-xt-relation ...
  print-xt-relation dataset xt.dat 52deg
*54.0
xt-plot angle 54.0 x-range 0.0 1.40 x-step 0.05 plot-xt-relation ...
  print-xt-relation dataset xt.dat 54deg
*56.0
xt-plot angle 56.0 x-range 0.0 1.40 x-step 0.05 plot-xt-relation ...
  print-xt-relation dataset xt.dat 56deg
*58.0
xt-plot angle 58.0 x-range 0.0 1.40 x-step 0.05 plot-xt-relation ...
  print-xt-relation dataset xt.dat 58deg
*60.0
xt-plot angle 60.0 x-range 0.0 1.40 x-step 0.05 plot-xt-relation ...
  print-xt-relation dataset xt.dat 60deg
```

```
*62.0
xt-plot angle 62.0 x-range 0.0 1.40 x-step 0.05 plot-xt-relation ...
  print-xt-relation dataset xt.dat 62deg
```

A.4.3 ARRIVAL

This data is displayed in Figure 4-1

```
& CELL
get vdc

& GAS
get argeth

& DRIFT
area  -1.5 -0.636  1.5 1.0
lines 60

* min-angle track

arrival electron 1 x-range 0.0 1.4 x-step 0.05 y-range -.21 .21 ...
  angle 47.34 plot-overview dataset argetharr.dat min


* mean-angle track

arrival electron 1 x-range 0.0 1.4 x-step 0.05 y-range -.21 .21 ...
  angle 54.74 plot-overview dataset argetharr.dat mean


* max-angle track

arrival electron 1 x-range 0.0 1.4 x-step 0.05 y-range -.21 .21 ...
  angle 61.52 plot-overview dataset argetharr.dat max
```

A.4.4 TIMING

The TIMING instuction is not discussed in the GARFIELD manual for Version 5.18 [15]. This instruction is available in this version, however, and is briefly discussed in the help facility available for Version 5.18. This file generates the drift-time spectrum shown in Figure 3-7.

```
& CELL
get vdc

& GAS
get argeth

& DRIFT

* drift-time spectrum for argon 62.9-ethane 37.1

lines 200
area  -1.5 -0.3  1.5 0.3
TIMING ELECTRON 1 x-range -1.45 0.0 angle-range 53.787 55.673  ...
   monte-carlo-loops 40000 plot-selected-electron time-window 0.0 0.30

& QUIT
```

Appendix B

Interpolation

B.1 Bilinear interpolation

B.1.1 Table of Data

The following table of x values, measured in cm, has been used. The table is made by interpolation of the xt-data output by `GARFIELD`, using the code given in section A.2.2. The table lists x values for angles of $\theta' = 46$-62, every two degrees, and for t-values of 0 to 270 nanoseconds. Note that toward the end of the table some values have been extrapolated outside the bondaries of the chamber. This has been done only to make a matrix that included all posible values inside the chamber, but these should not represent valid data points.

t(ns)	x_perp (cm) for angles:								
	46	48	50	52	54	56	58	60	62
0	0	0	0	0	0	0	0	0	0
1	0.0189	0.0198	0.0206	0.0214	0.0224	0.0236	0.0250	0.0264	0.0280
2	0.0280	0.0291	0.0303	0.0315	0.0329	0.0344	0.0361	0.0382	0.0408
3	0.0353	0.0366	0.0380	0.0397	0.0416	0.0438	0.0463	0.0494	0.0525
4	0.0422	0.0439	0.0457	0.0479	0.0503	0.0527	0.0554	0.0585	0.0622
5	0.0491	0.0510	0.0530	0.0553	0.0578	0.0606	0.0638	0.0675	0.0719
6	0.0555	0.0575	0.0598	0.0624	0.0653	0.0685	0.0722	0.0765	0.0815
10	0.0805	0.0836	0.0870	0.0908	0.0952	0.1001	0.1057	0.1119	0.1193
15	0.1117	0.1159	0.1207	0.1260	0.1319	0.1387	0.1464	0.1551	0.1652

```
 20 0.1426 0.1480 0.1541 0.1609 0.1686 0.1772 0.1870 0.1981 0.2112
 30 0.2039 0.2118 0.2205 0.2305 0.2418 0.2545 0.2689 0.2854 0.3046
 40 0.2628 0.2728 0.2842 0.2975 0.3116 0.3283 0.3483 0.3695 0.3962
 50 0.3172 0.3286 0.3416 0.3564 0.3723 0.3914 0.4127 0.4371 0.4647
 60 0.3675 0.3795 0.3931 0.4080 0.4251 0.4445 0.4663 0.4915 0.5197
 70 0.4151 0.4275 0.4412 0.4567 0.4738 0.4934 0.5152 0.5406 0.5692
 80 0.4617 0.4740 0.4878 0.5034 0.5206 0.5402 0.5621 0.5876 0.6163
 90 0.5074 0.5199 0.5336 0.5493 0.5666 0.5862 0.6081 0.6331 0.6624
100 0.5528 0.5653 0.5791 0.5947 0.6120 0.6317 0.6536 0.6788 0.7080
110 0.5980 0.6105 0.6244 0.6400 0.6573 0.6770 0.6989 0.7244 0.7533
120 0.6432 0.6557 0.6695 0.6851 0.7024 0.7218 0.7441 0.7696 0.7985
130 0.6883 0.7008 0.7146 0.7302 0.7474 0.7667 0.7892 0.8147 0.8436
140 0.7333 0.7458 0.7597 0.7753 0.7926 0.8123 0.8343 0.8597 0.8887
150 0.7784 0.7909 0.8048 0.8204 0.8377 0.8574 0.8794 0.9046 0.9337
160 0.8234 0.8357 0.8498 0.8654 0.8827 0.9022 0.9244 0.9499 0.9786
170 0.8685 0.8808 0.8948 0.9104 0.9278 0.9474 0.9695 0.9948 1.0237
180 0.9136 0.9260 0.9399 0.9555 0.9729 0.9926 1.0145 1.0400 1.0689
190 0.9586 0.9710 0.9849 1.0006 1.0179 1.0376 1.0596 1.0851 1.1139
200 1.0036 1.0162 1.0299 1.0456 1.0629 1.0827 1.1046 1.1301 1.1590
210 1.0487 1.0612 1.0750 1.0907 1.1080 1.1272 1.1497 1.1751 1.2040
220 1.0937 1.1063 1.1201 1.1357 1.1531 1.1723 1.1947 1.2202 1.2491
230 1.1388 1.1513 1.1652 1.1808 1.1981 1.2178 1.2398 1.2653 1.2941
240 1.1838 1.1964 1.2102 1.2258 1.2430 1.2629 1.2848 1.3103 1.3391
250 1.2289 1.2414 1.2552 1.2709 1.2882 1.3079 1.3299 1.3553 1.3841
260 1.2739 1.2865 1.3003 1.3159 1.3333 1.3529 1.3749 1.4003 1.4291
270 1.3190 1.3315 1.3454 1.3609 1.3784 1.3979 1.4199 1.4453 1.4741
```

B.1.2 Code

The following C code was used to perform the interpolation discussed in Section 4.1.2; this subroutine takes the angle θ (theta1) and the measured time (t1) and returns the corresponding x value.

```
#include <stdio.h>
#include <stdlib.h>

#define TDIM 35
#define THDIM 9
```

```
void locate(float [], unsigned long, float, unsigned long *);

float findx(float theta1, float t1)
{
  FILE *fpt, *fptheta, *fpxdata;

  int i,j;
  unsigned long jt, jth;
  float u,v;
  float x1,x2,x3,x4;
  float x, dx;
  float **x_data;
  float temp;

  float t[TDIM] = {0.0};
  float theta[THDIM] = {0.0};

  x_data = (float **) malloc (THDIM*sizeof(float*));
  for (i=0; i< TDIM ; ++i)
    x_data[i] = (float*) malloc(TDIM*sizeof(float));

  fpt = fopen("t", "r");
  for(i = 0; i < TDIM; i++){
    fscanf(fpt, "%f", (t+(i)) );
    }
  fclose(fpt);

  fptheta = fopen("theta", "r");
  for(i = 0; i < THDIM; i++){
    fscanf(fptheta, "%f", (theta+(i)) );
    }
  fclose(fptheta);

  fpxdata = fopen("nsxdata2", "r");
  for (i = 0; i < THDIM; i++){
    for (j = 0; j < TDIM; j++){
      fscanf(fpxdata, "%f", &temp);
      *(x_data[i]+j) = temp;
    }
  }
  fclose(fpxdata);

  locate(theta, THDIM, theta1, &jth);

  locate(t, TDIM, t1, &jt);
```

```
  v = (t1-t[jt])/(t[jt+1]-t[jt]);
  u = (theta1-theta[jth])/(theta[jth+1]-theta[jth]);

  x1 = *(*(x_data+jth)+jt);
  x2 = *(*(x_data+jth+1)+jt);
  x3 = *(*(x_data+jth+1)+jt+1);
  x4 = *(*(x_data+jth)+jt+1);

  x = (1-u)*(1-v)*x1+u*(1-v)*x2+u*v*x3+(1-u)*v*x4;

  return(x);
}

void locate(float xx[], unsigned long n, float x, unsigned long *j)
{
  unsigned long ju, jm, jl;
  int ascnd;

  jl=0;
  ju=n+1;
  ascnd=(xx[n-1] >= xx[0]);
  while (ju-jl > 1){
    jm=(ju+jl) >> 1;
    if (x >= xx[jm-1] == ascnd)
      jl=jm;
    else
      ju=jm;
  }
  if (x == xx[0]) *j=0;
  else if (x == xx[n-1]) *j=n-2;
  else *j=jl-1;
}
```

B.2 Interpolation with Higher Order Polynomials

If more accuracy is desired than the above method is able to provide, one can perform interpolation in two dimensions using a higher order polynomial, but the above method gives accuracy that is consistant with GARFIELD to as much accuracy as is possible with the chamber, thus this seems unnecessary. It is not recommend that a polynomial of

order of more than 3 or 4 be used. This method is discussed in Section 3.6 of *Numerical Recipes* [11], and is not given explictly here. The same data, given in A.2.1, may be used with this method; another table may be easily substituted.

Bibliography

[1] U. Becker *et al.* Gases for drift chambers in SSC/LHC environments. *Nuclear Instruments and Methods*, A315:14, 1992.

[2] W. Bertozzi *et al.* Focal plane instrumentation: A very high resolution MWPC system for inclined tracks. *Nuclear Instruments and Methods*, 141:457–476, 1977.

[3] W. Blum and L. Rolandi. *Particle Detection with Drift Chambers.* Springer-Verlag, New York, 1993.

[4] CEBAF. *Conceptual Design Report Basic Experimental Equipment*, April 13 1993.

[5] M. O. Distler. *Aufbau und Test einer vertikalen Driftkammer.* Diplomarbeit, Institut für Kernphysik, Mainz, July 1990.

[6] Hansjorg Fischle, Joachim Heintze, and Bernhard Schmidt. Experimental determination of ionization cluster size distributions in counting gases. *Nuclear Instruments and Methods in Physics Research*, A301:202–214, 1991.

[7] David V. Jordan. *A Separation of the Longitudinal and Transverse Structure Functions in the D(e,e'p)n Reaction.* PhD dissertation, Massachusetts Institute of Technology, Department of Physics, February 1994.

[8] F. Lapique and F. Piuz. Simulation of the measurement by primary cluster counting of the energy lost by a relativistic ionizing particle in argon. *Nuclear Instruments and Methods*, 175:297–318, 1980.

[9] Craig Leathers. *Efficiency Measurements on the CEBAF Hall A VDCs.* Undergraduate thesis, Massachusetts Institute of Technology, Department of Physics, June 1996.

[10] Donald H. Perkins. *Introduction to High Energy Physics.* Addison-Wesley, Reading, Massachusetts, Second edition, 1982.

[11] William H. Press, Brian Flannery, Saul Teukolsky, and William Vetterling. *Numerical Recipes in C.* Cambridge University Press, New York, second edition, 1992.

[12] John Ragland. *Constuction and Testing of a Prototype for the CEBAF Hall A VDC.* Undergraduate thesis, Massachusetts Institute of Technology, Department of Physics, June 1993.

[13] F. Sauli. Principles of operation of multiwire proportional and drift chambers. In *Lectures given in the Academic Training Programme of CERN 1975-1976*, Geneva, May 1977. CERN European Organization for Nuclear Research.

[14] Jeffrey A. Templon. *Continuum Nuclear Structure via* (p, p', X) *Reactions and Application to* ^{12}C. PhD dissertation, Indiana University, Department of Physics, April 1993.

[15] Rob Veenhof. *Garfield, a drift-chamber simulation program: User's guide.* CERN, Version 5.18, December 1995. The latest version of the manual is available in html at: http://consult.cern.ch/writeup/garfield/main.html or as a postscript file at: http://consult.cern.ch/writeup/garfield/main.ps.

[16] Rob Veenhof. Private communication.